Review

Dixon Techniques for Water and Fat Imaging

Jingfei Ma, PhD*

In 1984, Dixon published a first paper on a simple spectroscopic imaging technique for water and fat separation. The technique acquires two separate images with a modified spin echo pulse sequence. One is a conventional spin echo image with water and fat signals in-phase and the other is acquired with the readout gradient slightly shifted so that the water and fat signals are 180° out-of-phase. Dixon showed that from these two images, a water-only image and a fat-only image can be generated. The water-only image by the Dixon's technique can serve the purpose of fat suppression, an important and widely used imaging option for clinical MRI. Additionally, the availability of both the water-only and fat-only images allows direct image-based water and fat quantitation. These applications, as well as the potential that the technique can be made highly insensitive to magnetic field inhomogeneity, have generated substantial research interests and efforts from many investigators. As a result, significant improvement to the original technique has been made in the last 2 decades. The following article reviews the underlying physical principles and describes some major technical aspects in the development of these Dixon techniques.

Key Words: water and fat separation; Dixon imaging; phase correction; phase unwrapping; fat suppression; chemical shift imaging
J. Magn. Reson. Imaging 2008;28:543–558.

MR IMAGES ACQUIRED IN VIVO usually contain signals from both water and fat. In many pulse sequences, fat appears hyperintense. However, the contribution from water is often of the primary interest for many practical applications. Without suppression, the bright fat signal may result in aggravated motion-related artifacts and, more importantly, reduce the underlying lesion conspicuity. Because of its chemical shift, fat is also responsible for the well-known spatial misregistration artifacts, which can appear both along the frequency encode direction and along the slice select direction. For a few other applications such as diagnosis of bone marrow diseases or hepatic steatosis, detection rather than suppression of the fat signal can also be valuable.

Several approaches have been proposed and developed for achieving fat suppression. Perhaps the most popular is the chemical shift selective saturation (1) or its variants. In this approach, a frequency selective radiofrequency (RF) pulse and a spoiler gradient pulse are used in conjunction to first excite and then saturate the fat magnetization before water is excited for imaging. Alternatively, a frequency selective RF pulse can be used to directly excite only the water magnetization and leave the fat magnetization alone along the longitudinal axis. These techniques, particularly the selective saturation technique, are easy to implement and have been widely used with great success. However, both selective saturation pulses and selective excitation pulses increase the scan time. Another limitation for fat suppression by the selective saturation pulses is that it typically requires an accurate 90° flip angle, and as a result, its performance can be dependent on B1 homogeneity. Perhaps most importantly, fat suppression using the frequency selective approach requires that B0 magnetic field homogeneity be substantially less than the water/fat chemical shift difference (which is 3.5 ppm or 220 Hz at 1.5 Tesla) within the entire imaging field of view (FOV). While such a requirement is usually within a scanner's technical specifications, the actual magnetic field achievable is often compromised after a patient is placed into the scanner. In routine practices, obtaining consistent and satisfactory fat suppression using the frequency selective approach remains a challenge, particularly for imaging off-isocenter, with large FOV, or anatomies with strong susceptibility effects.

Fat suppression can also be achieved with short-tau inversion recovery (STIR) imaging (2). In STIR, the longitudinal magnetization of fat is first flipped 180° by an inversion pulse and then allowed to relax back to its equilibrium along the magnetic field direction. Water magnetization, which is usually also flipped 180° by the same inversion pulse, is excited for imaging when the longitudinal magnetization of fat crosses the null point. Because fat has a characteristically short T1 relaxation (approximately 150 ms at 1.5 Tesla), water has usually relaxed only partially along the longitudinal axis at the time of the excitation. Compared with the frequency-selective approach, STIR has a major advantage of being insensitive to the B0 magnetic field inhomogeneity, as well as to the B1 inhomogeneity when adiabatic

Department of Imaging Physics, The University of Texas M.D. Anderson Cancer Center, Houston, Texas.
Contract grant sponsor: The Bracco/RSNA Research Scholar Award; Contract grant sponsor: The Susan Komen Breast Cancer Foundation.
*Address reprint requests to: J.M., Department of Imaging Physics, The University of Texas M.D. Anderson Cancer Center, 1515 Holcombe Blvd., Houston, TX 77030. E-mail: jma@di.mdacc.tmc.edu
Received April 16, 2008; Accepted June 6, 2008.
DOI 10.1002/jmri.21492
Published online in Wiley InterScience (www.interscience.wiley.com).

inversion pulses are used. Intrinsic limitations of STIR, however, include its reduced signal to noise ratio (SNR) and reduced scan time efficiency (due to the inclusion of the inversion pulses). Additionally, STIR may inadvertently suppress tissues of interest that have short longitudinal relaxation times. To alleviate the problem, the STIR inversion pulses can be designed to be spectrally selective of only the fat magnetization. However, such modification will inevitably render the technique sensitive to the B0 magnetic field inhomogeneity.

The third approach for achieving fat suppression is the simple spectroscopic imaging technique that was originally published by Dixon (3). This technique and its many later variants by other investigators are the subject of this review. As for the frequency selective approach, the Dixon techniques rely on the water/fat chemical shift difference. However, the Dixon techniques encode the chemical shift difference into the signal phase with a modified data acquisition and then achieve the water/fat separation through postprocessing. In its original implementation, Dixon acquired an image with water and fat signals in-phase and another image with water and fat signals 180° out-of-phase. Dixon showed that simple summation and subtraction of the two images can yield a water-only image and a fat-only image, respectively. Quite generally, this simple spectroscopic imaging concept can potentially be used for fat suppression or fat quantification in many different types of pulse sequences or for many different clinical applications.

Several major challenges for the Dixon techniques, however, have hindered their widespread use. First and foremost, B0 inhomogeneity, which is a major problem for fat suppression by the frequency selective approach, appears as phase errors in the acquired Dixon images. Without proper phase correction, the simple summation and subtraction approach as originally proposed by Dixon results in incomplete water and fat separation, thus making the Dixon techniques also sensitive to the magnetic field inhomogeneity. Second, substantially increased minimum total scan time was needed to acquire multiple images for proper postprocessing. Furthermore, a Dixon data acquisition often requires pulse sequence timing changes to induce the desired water/fat relative phase changes in the acquired images. In the presence of motion and for finite tissue relaxation times, the increased scan time and the changes to the pulse sequence timing can both lead to noticeable degradation in the quality of the acquired images. As a result, the processed water-only and fat-only images will suffer from the same image quality degradation, such as increased motion artifacts or increased image blurring.

Despite these challenges, substantial improvement and technical advances have been made in the past 2 decades for realizing the potentials of the Dixon techniques. Much of the research has been focused on developing improved phase correction (through postprocessing algorithms, data acquisition, or a combination of both) so that the B0 inhomogeneity effects can be removed and the water/fat separation can be achieved reliably. Methods have also been proposed and successfully implemented to address the scan time and the image quality issues from a Dixon acquisition. With these developments, it is now possible to successfully apply a Dixon technique in a routine clinical setting to such important and demanding applications as the dynamic imaging of abdomen after intravenous injection of contrast agent. Figure 1 shows an example of this application where the water-only images at the arterial (Fig. 1a) and delay-enhancement (Fig. 1b) phase were acquired in a breath-hold time with a three-dimensional (3D) fast spoiled gradient echo dual-echo Dixon technique (4). Image quality and fat suppression of these water-only images compare very favorably to an image (Fig. 1c) that was acquired of the same patient and with identical scan parameters using a state-of-the-art 3D fast spoiled gradient echo technique with a conventional frequency selective fat suppression. Because some major MR vendors have recently begun to introduce the Dixon techniques into their product offering, we anticipate that the clinical applications of the Dixon techniques will be greatly expanded in the next few years. In the following, we will provide a brief overview of the underlying physical principles and describe some major technical aspects in the development of the Dixon techniques.

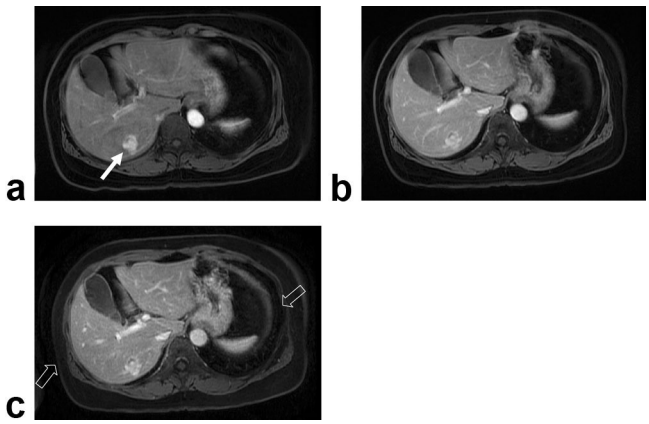

Figure 1. a,b: The water-only images at the arterial (a) and delay-enhancement (b) phase of a patient after intravenous injection of gadolinium-based contrast agent. These images were acquired in a routine clinical setting and in breath-hold time with a 3D fast spoiled gradient echo dual-echo Dixon technique. **c:** An image of the same patient and of identical scan parameters acquired at the delayed enhancement using a 3D fast spoiled gradient echo technique with a conventional frequency selective fat suppression. The liver lesion (hemangioma, solid arrow) was well depicted in the Dixon images. Suboptimal fat suppression by the conventional fat suppression toward the peripheral of the FOV is indicated by the block arrows. (Images courtesy of Dr. Russell Low, Sharp and Children's MRI Center, San Diego, CA.)

SIGNAL MODEL

It is important to have a clear understanding of the signal models for the correct processing and interpretation of the Dixon images. A fundamental assumption of most Dixon techniques is that water and fat are the only two signal-contributing chemical species in the object to be imaged. Under this assumption, the com-

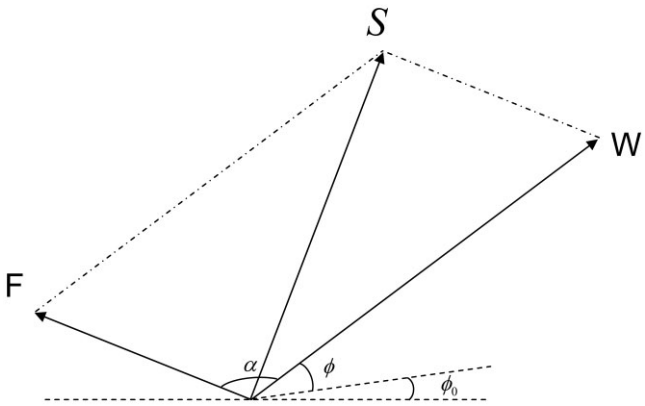

Figure 2. A vector representation of the complex signal *S* as given in Equation [1] for a given pixel with two spectral components, water (*W*) and fat (*F*). α is the phase angle of fat relative to that of water due to their chemical shift difference. ϕ is the error phase due to the magnetic field inhomogeneity and ϕ_0 is another error phase due to other system imperfections such as the spatial dependence of RF penetration and different signal delay in the receiver chains. In a Dixon acquisition, a time delay is introduced in the pulse sequence to achieve a desired value of α according to the postprocessing algorithm used. Successful phase correction is a prerequisite for a Dixon technique and can be very challenging because ϕ changes concurrently with α. (Reprinted from Ma (44) with permission of Wiley-Liss, Inc, a subsidiary of John Wiley & Sons.)

plex image after the Fourier transform of the acquired data can be expressed as follows:

$$S(x,y) = [W(x,y) + F(x,y) \cdot e^{i\alpha}] \cdot e^{i\phi(x,y)} \cdot e^{i\phi_0(x,y)} \quad [1]$$

where (x,y) represents the spatial coordinates (or indices) of a pixel. *W* and *F* are in general real and nonnegative numbers representing the magnitudes of the magnetizations at a given pixel for water and fat, respectively. α is the phase angle of fat relative to that of water due to their chemical shift difference, ϕ is the error phase due to the magnetic field inhomogeneity, and ϕ_0 is another error phase due to other system imperfections such as the spatial dependence of RF penetration and different signal time delay in the receiver chains. Figure 2 illustrates graphically the vector relationship between the various quantities in Equation [1]. In a Dixon acquisition, Δt, which represents changes in echo time (TE) or time shifts from a spin echo, is often introduced in a pulse sequence to effect certain desired values of α. As a result, α is proportional to Δt, that is:

$$\alpha = \gamma \cdot B_0 \cdot \sigma \cdot \Delta t \quad [2]$$

where γ is the proton gyromagnetic ratio, σ is the chemical shift of fat relative to water, and B_0 is the externally applied magnetic field. The error phase ϕ, which is due to the magnetic field inhomogeneity, is also proportional to Δt:

$$\phi = \gamma \cdot \Delta B_0 \cdot \Delta t \quad [3]$$

where ΔB_0 represents the magnitude of the magnetic field inhomogeneity.

Several comments need to be made regarding Equations [1–3]. First, *W*, *F*, ϕ, and ϕ_0 in Equation [1] and ΔB_0 in Equation [3] are all spatially dependent and thus may vary from pixel to pixel. While changes in ΔB_0 in principle affect α as well, the magnitude of ΔB_0 is much smaller than B_0. Thus, α can be considered spatially invariant and depends only on Δt and the chemical shift of fat (see Eq. [2]), which is a constant. When multiple receiver coils are used, *W* and *F* may be weighted by each coil's spatial sensitivity and ϕ_0 is usually also coil dependent. In contrast, ϕ is determined by the magnetic field inhomogeneity (see Eq. [3]) and, therefore, should be constant for all the coils. Second, *W* and *F* are the magnitudes of the water and fat magnetizations at the time of the sampling. In addition to their respective proton densities, they are, therefore, in general dependent on other tissue properties (e.g., relaxation times T2, T2*, T1, and diffusion constant) as well as the pulse sequence and scan parameters (e.g., TR, TE, and diffusion weighting) used for the data acquisition. For the same reason, *W* and *F* may also be dependent on Δt, particularly when T2* is very short, even though Δt is usually quite small (in the order of a few milliseconds). Third, Equation [1] assumes implicitly that water or fat each has only a single spectral peak. While this assumption is generally true for water, fat is known to contain many spectral components (5). Furthermore, each individual spectral component of fat has its own relaxation times, and some spectral peaks are even modulated with scalar coupling. Despite these complexities, the main contributors to the fat spectrum have been identified as the methylene and a few other proton species (e.g., the terminal methyl protons) whose resonance frequencies are clustered around a location that is approximately 3.5 ppm away from the resonance frequency of water. Another noticeable contributor to the fat spectrum is the olefinic proton whose resonance frequency falls very close to that of water (with a separation of only approximately 0.5 ppm). The presence of these multiple spectral components would in general result in a complex magnetization for fat at a given Δt rather than that represented by a real and nonnegative number in Equation [1]. For practical purposes, however, Equation [1] is a good approximation because the fat spectrum can be modeled as consisting of two broadened peaks, with one being shifted by 3.5 ppm from the water and another at the water resonance (even though the actual location of the major olefinic peak is approximately 0.5 ppm away from the water resonance). Pixels containing even only fat tissues will thus in general have signal contributions to both the "water-only" image and the "fat-only" image. A combined T2 or T2* can be used to account for the spectral broadening due to the presence of the multiple peaks and the intrinsic T2 or T2* relaxation. Because each individual spectral component has different relaxation times, however, the relative contribution of the "water" component and the "fat" component and their combined T2 or T2* can all be pulse sequence or scan parameter dependent.

The primary objective of the Dixon techniques is to determine W and F from an acquired image or images that are represented by S in Equation [1]. While not considered here and thereafter in this review, it is recognized that determination of the field inhomogeneity or tissue relaxation maps may also be useful for certain applications. In a typical Dixon technique, images are acquired with a specific set of Δt to induce a desired set of α. As a convention, a technique is referred to as a two-point Dixon technique when two images are acquired and used in the postprocessing. Similarly, a three-point Dixon technique refers to a technique that acquires three images for postprocessing. In addition, a technique may be referred to by the set of the α values used. For example, the original Dixon technique acquired two images with one being in-phase ($\alpha = 0$) and another being 180° out-of-phase ($\alpha = 180°$). Therefore, the technique can be referred to as a two-point Dixon technique with (0, 180°) or (0, π) acquisition. The technical development of the Dixon techniques consists largely of the many different sampling strategies as well as different postprocessing strategies for improved water and fat imaging.

THE ORIGINAL TWO-POINT DIXON TECHNIQUE

As mentioned above, the original two-point Dixon technique (3) acquires two images with a (0, 180°) sampling strategy, which can be written as:

$$S_0 = (W + F) \cdot e^{i\phi_0} \quad [4]$$

$$S_1 = (W - F) \cdot e^{i\phi} \cdot e^{i\phi_0} \quad [5]$$

Note hereafter, we will choose to leave out the explicit dependence of W, F, ϕ, and ϕ_0 on the spatial coordinates (x, y) for simplicity. From Equations [4] and [5], W and F can be determined directly when ϕ is zero:

$$W = 0.5 \cdot |S_0 + S_1| \quad [6]$$

$$F = 0.5 \cdot |S_0 - S_1| \quad [7]$$

where $|\cdots|$ represents the operation of taking the absolute value. Note that because of the absolute value operation, the solution given by Equations [6] and [7] is not affected by the error phase ϕ_0, even though ϕ_0 is in general spatially variant.

When ϕ is not zero, Equations [6] and [7] do not provide a clean water and fat separation and the water-only image or the fat-only image will in general contain admixture of both water and fat. To remedy the problem, Dixon proposed to form two magnitude images of $|S_0|$ and $|S_1|$ before they are summed or subtracted as in Equations [6] and [7]. However, it is easy to see that the water-only image thus obtained is really just an image where every pixel contains the dominant signal of the corresponding pixel, which can be either water or fat, rather than only water. Likewise, the fat-only image thus obtained is just an image where every pixel contains the least dominant signal of the corresponding pixel. Reliable and consistent water/fat separation for an entire image and the success of the two-point Dixon technique are, therefore, affected by the presence of ϕ, which in turn is directly related to the magnetic field inhomogeneity (Eq. [3]). Nonetheless, it is interesting to note that by taking the absolute value of the images before summation or subtraction, the water and fat separation is actually already correct on a pixel level without the need to know the actual phase errors. The real problem is thus in making a correct binary choice on whether the summed or the subtracted result corresponds to the water or fat on a pixel level.

THE THREE-POINT DIXON TECHNIQUES

After Dixon's original work, Yeung and Kormos (6), Glover and Schneider (7), and Glover (8) showed that it is actually possible to determine ϕ by acquiring an additional image. The modified acquisition scheme with an additional image used was in the form of either (−180°, 0, 180°) or (0, 180°, 360°). In the case of (−180°, 0, 180°), the image with the −180° phase was acquired in a spin echo pulse sequence by shifting the refocusing RF pulse with an equal amount but in the opposite direction relative to the conventional spin echo position as for the image with the 180° phase. Using the same notations as for Equations [4] and [5], we can write the image with the −180° phase as:

$$S_{-1} = (W - F) \cdot e^{-i\phi} \cdot e^{i\phi_0} \quad [8]$$

Because W and F are real and nonnegative numbers, ϕ can be calculated from Equation [5] and Equation [8] as:

$$\hat{\phi} = 0.5 \cdot \arg[S_1 \cdot S^*_{-1}\} \quad [9]$$

where arg represents arctangent for extracting the phase of a complex number and * represents taking the complex conjugate. Note that the multiplication of S_1 and S^*_{-1} effectively removes the contribution due to both ϕ_0 and the possible sign change in (W–F).

In the case of the (0, 180°, 360°) acquisition scheme, the image with the 360° phase can be acquired by doubling the time shift in the same direction as for the image with the 180° phase. Because water and fat are again in-phase when their phase angle is 360°, the corresponding image can be written as:

$$S_2 = (W + F) \cdot e^{i2\phi} \cdot e^{i\phi_0} \quad [10]$$

Combining Equation [4] and Equation [10], we can calculate ϕ as:

$$\hat{\phi} = 0.5 \cdot \arg\{S_2 \cdot S^*_0\} \quad [11]$$

Clearly, if ϕ is determined correctly (i.e., $\phi = \hat{\phi}$) from either Equation [9] or Equation [11], the magnetic field inhomogeneity effects can be removed from the signal equations. Following that, W and F can be determined using simple summation and subtraction as in the original Dixon technique.

A major complication arises from a seemingly very simple limitation that the arg operation in Equation [9] or Equation [11] can determine the phase of its argument only within the range of $-\pi$ to π. When the true phase of the argument is smaller than $-\pi$ or greater than π, a multiple of 2π will be automatically added/subtracted to the true phase so that the calculated phase falls back within the range of $-\pi$ to π. Such phase wrapping has a direct consequence on the subsequent water and fat separation. If the calculated phase is shifted by 2π from the true phase, for example, $\hat{\phi}$ will differ from ϕ by π (because of the multiplication by 0.5 in Equation [9] or Equation [11]). As a result, S_1 or S_{-1} after the removal of the $e^{i\phi}$-term will differ from their true value by a factor of -1, and the solution of W and F will thus be interchanged. Without knowing where phase wrapping has occurred, this presents a dilemma similar to that encountered in the original two-point Dixon technique when taking the absolute value of the in-phase and out-of-phase images before the summation and subtraction. To avoid the ambiguity, we must either require that no phase wrapping occurs or be able to detect the phase wrapping and unwrap the phase when phase wrapping is present. Equation [3] indicates that phase wrapping will occur when the field inhomogeneity is more than half the chemical shift difference between water and fat, or approximately 1.75 ppm. Such a requirement on the field inhomogeneity is essentially the same as that for the successful fat suppression by the frequency selective methods and, as discussed, is difficult to achieve in many clinical situations. Therefore, correct water and fat separation using the Dixon approach has been deemed to rely largely on the success of phase unwrapping.

PHASE UNWRAPPING

Phase unwrapping is a well-studied but long-standing problem outside the field of MRI (e.g., in synthetic aperture radar interferometry). Although many different methods of phase unwrapping have been developed (see, e.g., Ghiglia and Pritt) (9), no general solution is available, particularly in the context of MRI. Mathematically speaking, phase unwrapping can be stated simply as recovering the true phase ϕ from its principal or wrapped value $\hat{\phi}$:

$$\phi = \hat{\phi} + k \cdot 2\pi \qquad [12]$$

where k is an integer and, as explained above, $\hat{\phi}$ is limited to a range between $-\pi$ and π and is determined from ϕ through a wrapping operator as follows:

$$\hat{\phi} = W[\phi] \qquad [13]$$

Phase unwrapping is not meaningful for an isolated image pixel because any multiples of 2π can be added to its principal value. Thus, phase unwrapping is in general only considered for an ensemble of pixels for which the true underlying phase is assumed to be spatially continuous or smooth. Under this assumption, phase wrapping results in discontinuities of $k \cdot 2\pi$ in the principal values of the phase between two neighboring pixels. The discontinuities are often called "fringelines" in two dimensions (9). The basic idea of phase unwrapping is to identify the fringelines and restore the spatial smoothness in the unwrapped phase by adding or subtracting appropriate multiples of 2π. It can be shown that the true underlying phase can always be recovered from the wrapped phase by integrating the wrapped difference (between the two neighboring spatial locations) of the wrapped phase as long as the following condition is met:

$$-\pi < \Delta\phi(x) \leq \pi \qquad [14]$$

where $\Delta\phi(x) = \phi(x + 1) - \phi(x)$ defines the *true* phase difference between two neighboring pixels. Conversely, it can also be shown that the true underlying phase cannot be recovered from the wrapped phase and phase unwrapping (by integrating the wrapped difference of the wrapped phase) will in general be incorrect when Equation [14] is not satisfied. Nevertheless, the results from the phase unwrapping will be smooth in the sense that the difference of the retrieved phase satisfies Equation [14] (even though the difference of the true underlying phase does not, a fact that is not known a priori from only the wrapped phase).

In MRI, spatial undersampling of the phase can lead to violation of the condition in Equation [14]. When magnetic field inhomogeneity is large and spatial resolution of an image is insufficient due to undersampling, the signal phase due to the field inhomogeneity can vary by more than π between two neighboring pixels. A more common source that can lead to violation of Equation [14] is noise and artifacts (e.g., due to motion or blood flow), for which phase may be purely random or unrelated to the underlying signal. An extreme case exists in regions of complete signal void (e.g., background regions). For those pixels, the measured phase does not provide any information on the true underlying phase (due to, for example, the magnetic field inhomogeneity). Although it may still be mathematically correct, phase unwrapping in those pixels is thus meaningless. Depending on the design of a specific algorithm, however, an error in phase unwrapping of those pixels may potentially affect and corrupt phase unwrapping in other regions where true phase is meaningful and must be determined.

Regardless of the underlying causes, violation of the condition in Equation [14] generates some singularities called residues or poles in a phase map (9,10). A residue or pole is defined as a 2×2 pixel loop around which an integration of the wrapped phase difference is not zero and is equal to a multiple of 2π. Existence of poles leads to a dilemma whereby phase unwrapping from one pixel to another pixel by integration becomes path dependent (Fig. 3). To ensure path independence, all the poles need to be first identified either explicitly or implicitly and then properly handled during the integration. Path-following methods fall into this general category of phase unwrapping. Another general but different category of methods for phase unwrapping is the minimum-norm methods. The general idea behind the minimum-

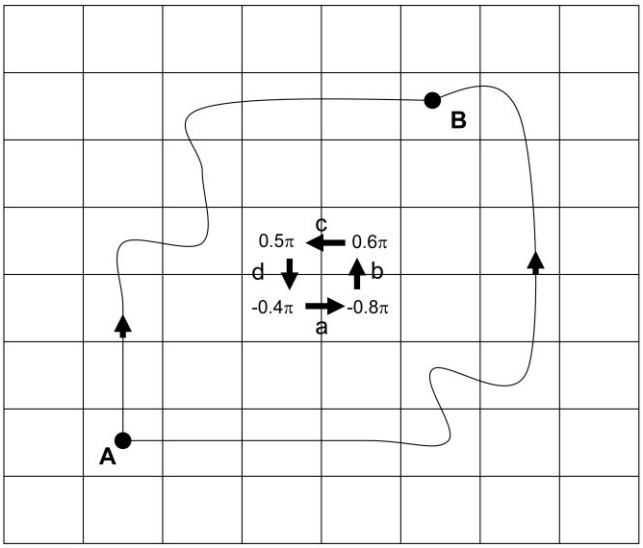

Figure 3. Poles or residues are identified as a 2 × 2 pixel loop in a phase map around which the sum of the wrapped phase difference is nonzero. A pole can be either positive or negative depending on the sign of the sum. The loop a–b–c–d is a negative pole because the sum of the wrapped phase difference is $W(-0.4\pi) + W(1.4\,\pi) + W(-0.1\,\pi) + W(-0.9\,\pi) = (-2\,\pi)$. The presence of poles makes phase unwrapping from one pixel (Point A) to another pixel (Point B) by integration potentially path dependent. To ensure path independence, the positive and negative poles enclosed by two different paths (e.g., along the two connecting lines between A and B) must be balanced.

norm methods is to unwrap the phase by minimizing some cost functions. Both the minimum-norm and the path-following methods for phase unwrapping have been used for Dixon imaging and will be briefly reviewed in the following.

Minimum-norm Methods

In the minimum-norm methods, phase unwrapping is achieved by requiring that the local derivative of the true phase (unknown) and the derivative of the wrapped phase (measured and known) match "as closely as possible." Perhaps the simplest and most-used minimum-norm method for phase unwrapping is by solving the least-squares problem (or L^2-problem, as it is mathematically known). The L^2-problem for phase unwrapping can be formulated as minimizing the sum of the squared difference between the derivative of the sought-after phase and the derivative of the measured phase. Obviously, such a cost function can be either weighted or unweighted with some chosen function (e.g., the amplitude of the signal). Furthermore, the L^2-formulation can be extended to a more generalized L^p-formulation, where $p \neq 2$.

For continuous variables, the unweighted L^2-problem can be reduced to a problem of solving the Poisson's equation (9):

$$\nabla^2\phi = \rho \qquad [15]$$

where ∇^2 is the Laplacian operator and ρ is a function that can be calculated directly from the measured phase. Equation [15] can be solved either directly or iteratively provided certain geometric boundary conditions are specified. Song et al reported applying this approach to processing a set of three-point Dixon data in MRI (11). Although the method is successful to some extent, it runs into difficulty in regions where the image SNR is low or the phase-unwrapping condition in Equation [14] is not satisfied. Therefore, Equation [15] can be solved reliably only in some reduced regions for which inconsistent pixels are masked out.

A more practical minimum-norm approach is to unwrap the phase through some empirical modeling of the true phase. For Dixon imaging, a polynomial model or truncated Taylor series is reasonable in some situations and has been used to represent the spatial phase variations (12,13). By imposing a specific model, phase unwrapping in the minimum-norm sense amounts to some parameter estimation. A major advantage of the model-based minimum-norm method is that the overall phase-unwrapping result is usually not affected by local regions of noise or phase inconsistency. Even for regions that are separated by large regions of signal voids, a model-based minimum-norm method can perform well. A major limitation of the methods lies in the fidelity of the empirical model that is used. When the residual phase (the difference between the model predicted phase and the true phase for a pixel) is greater than π, phase unwrapping for the pixel will be incorrect. To have a more accurate modeling, more parameter terms are needed in the polynomials or the Taylor series. However, such an approach increases the computational complexity and decreases the robustness of the model fitting. Most importantly, it is very difficult to use polynomials or Taylor series to accurately represent rapid and local variations in the true phase distribution.

Path-following Methods

A residue or pole in a phase map can be either positive or negative depending on whether the closed loop integration of the wrapped phase difference is positive or negative (Fig. 3). Path-following methods for phase unwrapping seek to define an integration path for phase unwrapping that does not enclose poles or encloses only equal number of positive and negative poles (9). There are in general two different approaches for the path-following methods. One is to explicitly identify all the residues or poles in the phase map and then to place "branch cuts," which are lines that connect two residues with different polarity. The integration path of phase unwrapping is prevented from crossing the "branch cuts." Properly placed "branch cuts" will thus avoid enclosing unbalanced poles and ensure the uniqueness of the phase unwrapping (9,10). The other approach of the path-following methods does not aim to generate explicit "branch cuts." In fact, it is not even necessary to identify the location of the residues. Instead, the integration path is guided or defined through some quality map, such as the phase derivatives. The idea behind the approach is that an integration path that is guided by a properly chosen quality map will be

able to implicitly avoid enclosing any unbalanced poles (9).

The explicit "branch cuts" approach for phase unwrapping was first proposed by Goldstein et al (14). The identification of the poles or residues on a phase map is easy and straightforward according to the definition of the poles. The real challenge lies in the placement of the "branch cuts." According to the approach by Goldstein et al, neighboring residues of opposite polarity are balanced in pairs with "branch cuts." Single residues are considered balanced when they are connected with "branch cuts" to the image boundary. The "branch cuts" generated by the Goldstein method essentially aim at minimizing the total length of the branch cuts, a condition that is implicitly assumed to be optimal for the branch cut placement. Under this assumption, several other modifications to the Goldstein's algorithm have also been proposed for more effective and proper placement of the "branch cuts" (9).

The advantage of an explicit branch cuts method is that once branch cuts are generated, the phase unwrapping results are guaranteed to be unique and independent of the integration path. A limitation of the approach is that there is no guarantee that the placement of the branch cuts by any algorithm is truly optimal or correct. As discussed above, poles and residues may arise from different causes (e.g., undersampling or noise), and thus they may have different characteristics. It is, therefore, conceivable that minimizing the total length of the branch cuts alone may not always lead to the correct placement of the branch cuts. On the basis of their study of some phase maps in MRI, Chavez et al (10) postulated that poles that are spatially close together are noise related and that longer-range poles are from true undersampling. Under this assumption, Chavez et al designed a fringeline tracking algorithm to distinguish between the two types of the poles based on their relative fringeline lengths. In the algorithm, noise poles of different polarities are paired up and easily taken care of. However, generation of the branch cuts for the long-range poles requires repeated application of the same fringeline tracking algorithm with different global phase offsets. Fringelines that stay relatively unchanged at the different global phase offsets are assumed as the branch cuts for the long-range poles. In comparison to the original Goldstein's algorithm, the algorithm by Chavez et al distinguishes two different types of poles that may exist in an MR image. However, the assumption that the two different types of the poles have different fringeline lengths is empirical, and hence there is still a fundamental limitation of not knowing whether the placement of the branch cuts is truly optimal.

An alternative path-following method for phase unwrapping is to use a carefully chosen quality map as a guide to determine the integration path without an explicit placement of branch cuts or even without any direct identification of the residues (9). As stated above, the idea behind this approach is that a properly selected quality map can guide the integration path so that it will implicitly avoid enclosing any unbalanced residues. In theory, there is also no guarantee that a quality map-guided integration will be able to follow a path that avoids enclosing unbalanced poles. However, selection of a quality map can be quite flexible, and phase unwrapping from a quality map-guided path-following method has been found to be surprisingly robust for many practical applications. The reason for the success of this method is that poles or residues tend to occur for pixels with low-quality values. In contrast, pixels with high-quality values usually are free of residues. As a result, phase unwrapping in properly chosen high-quality regions can be performed first with greater reliability and without corrupting phase unwrapping in other regions.

The actual implementation of a quality map guided path-following method is often similar to the implementation of the more general region growing. Although many different region-growing algorithms have been proposed, they usually contain three basic aspects that are critically important to the success of the final result: the selection of the initial seed, the selection and use of the quality map, and the criteria for phase unwrapping integration at each step of the region growing. Ideally, an algorithm should be fully automated and widely applicable, and the results should be reliable in the presence of noise and artifacts. In reality, different algorithms always contain certain assumptions that may be invalid under some specific situations. Therefore, there is no absolute guarantee that an algorithm will always generate the correct phase unwrapping results.

Szumowski et al first described the detailed implementation of a region growing-based approach for phase unwrapping in a three-point Dixon technique (15). The general scheme of the implementation is illustrated in Figure 4. According to their implementation, the initial seed pixel is selected manually in a region of good SNR. As part of the quality map construction, the phase map before phase unwrapping is first masked with an empirically chosen signal intensity threshold. Pixels designated as noise after thresholding are excluded from the processing. The region growing proceeds from the initial seed pixel by comparing the phase difference between the seed and the neighboring pixels. If the phase difference is less than an empirically chosen threshold $\Delta\Psi$ (e.g., $\pi/8 \sim \pi/4$), the neighboring pixel will retain its phase, is added to a pixel stack, and will be later used as a new seed pixel. If the phase difference is larger than $\Delta\Psi$, the phase of the neighboring pixel is added or subtracted by 2π. The difference between the resulting phase and the phase of the seed pixel is then recalculated. If the new difference is larger than $\Delta\Psi$, the pixel will retain its original phase before the 2π addition or subtraction and will not be added to the pixel stack as a new seed. If the difference is less than $\Delta\Psi$, the pixel will be deemed phase-unwrapped with the new phase after the 2π addition or subtraction and will be added to the pixel stack as a new seed. This process continues until all the pixels on the pixel stack have served as a seed pixel and no new pixels can be added to the pixel stack.

The algorithm by Szumowski et al is easy to implement and has been used successfully in many applications. However, a serious limitation with the approach is that both the angular threshold $\Delta\Psi$ and the signal intensity thresholding are empirical. The signal inten-

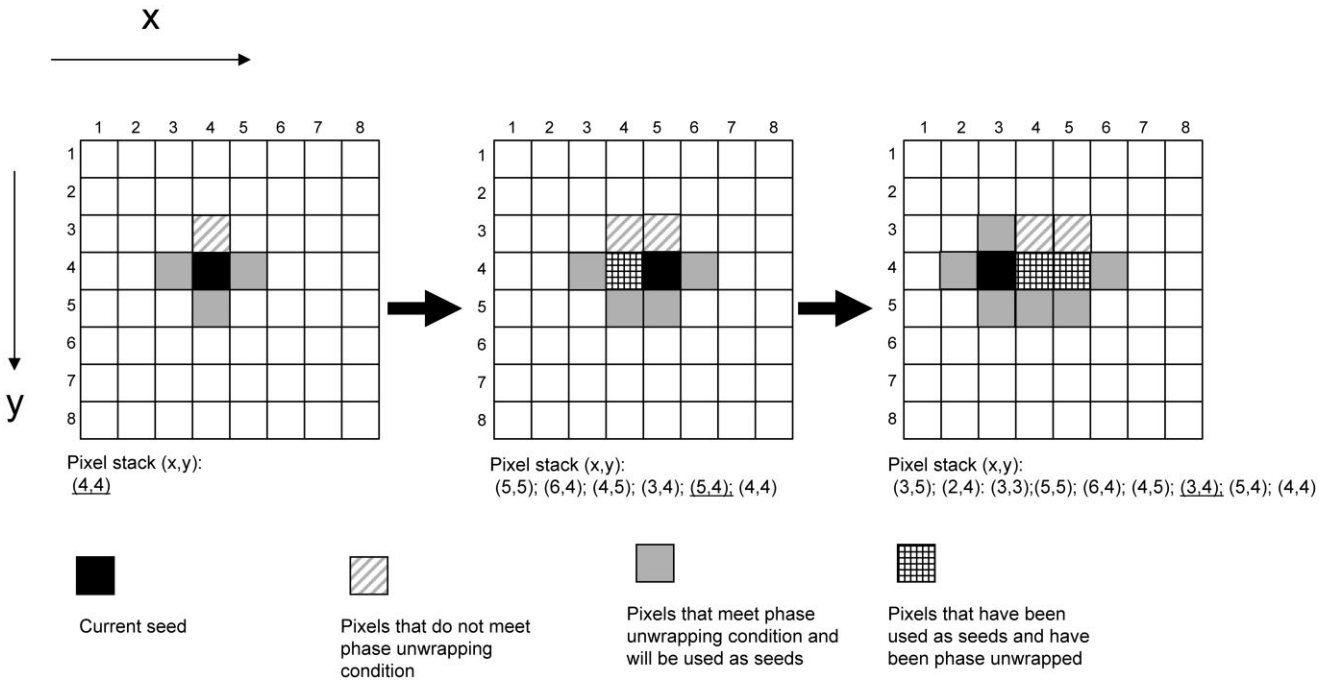

Figure 4. The region-growing algorithm by Szumowski et al (15) for phase unwrapping in a three-point Dixon technique. The region growing starts from a manually selected initial seed pixel and uses a pixel stack to track and guide the sequence of the region growing. At each seed pixel, the phase difference with its four nearest neighbors is computed and compared against an empirically determined angular threshold $\Delta\Psi$. A pixel will be unwrapped, placed onto the pixel stack, and used as a future seed if the phase difference is less than $\Delta\Psi$. Otherwise, phase unwrapping will not be performed and the pixel will not be placed onto the pixel stack. The pixel stack will be populated and de-populated during the region-growing process until the pixel stack is empty and the region growing stops. (Reprinted from Szumowski et al (15) with permission of the Radiological Society of North America [RSNA].)

sity thresholding may segment an image into multiple isolated regions, which can be difficult to handle by a region growing-based algorithm. The choice of $\Delta\Psi$ is perhaps even more challenging and difficult. When $\Delta\Psi$ is too small, the region growing may be terminated prematurely without unwrapping a large number of pixels. If $\Delta\Psi$ is too large, phase unwrapping may become erroneous. Because pixels that are placed onto the pixel stack are used as new seeds sequentially in a first-in and first-out (FIFO) basis, erroneous phase unwrapping at one single step can corrupt phase unwrapping of all the subsequent pixels.

Pixel-based Analytical Methods

Under certain conditions, it is actually possible to separate water and fat for the three-point Dixon data without phase unwrapping. One method that can achieve an analytical solution on a pixel basis is direct phase encoding (DPE) (16). In DPE, three sets of images are collected at three different water/fat relative phase angles of (α_0, $\alpha_0 + \alpha$, $\alpha_0 + 2\alpha$), where $\alpha \neq 180°$. Without losing generality and assuming $\alpha_0 = 0$, the three corresponding images can be written as:

$$S_0 = (W + F) \cdot e^{i\phi_0} \quad [16]$$

$$S_1 = (W + e^{-i\alpha}F) \cdot e^{-i\phi} \cdot e^{i\phi_0} \quad [17]$$

$$S_2 = (W + e^{-i2\alpha}F) \cdot e^{-i2\phi} \cdot e^{i\phi_0} \quad [18]$$

If two new complex variables are introduced as:

$$X = W \cdot e^{i\phi_0} \cdot e^{i\phi} \quad [19]$$

$$Y = F \cdot e^{i\phi_0} \cdot e^{i\phi} \cdot e^{i\alpha} \quad [20]$$

It is easy to see that if X and Y are determined, W and F are simply their magnitudes and can be derived by taking the absolute value of X and Y. To determine X and Y, Equations [16]–[18] can be manipulated mathematically into a quadratic equation in X or Y, which leads to two sets of possible solutions as follows:

$$\begin{cases} X_1 = \frac{1}{2}(S_0 + \Delta S) \\ Y_1 = \frac{1}{2}(S_0 - \Delta S) \end{cases} \quad [21]$$

$$\begin{cases} X_2 = \frac{1}{2}(S_0 - \Delta S) \\ Y_2 = \frac{1}{2}(S_0 + \Delta S) \end{cases} \quad [22]$$

where

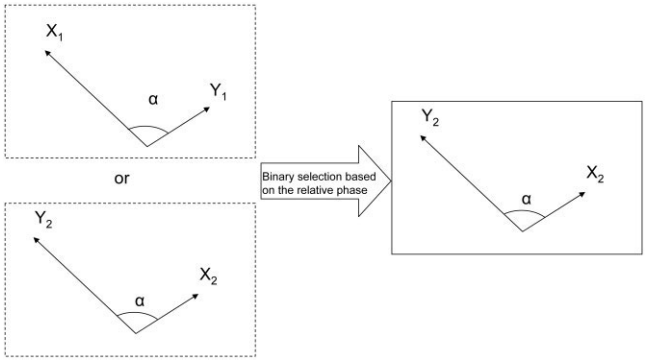

Figure 5. Direct phase encoding by Xiang and An (16). From the complex signals sampled at (α_0, $\alpha_0 + \alpha$, $\alpha_0 + 2\alpha$), two possible algebraic solutions for X and Y can be directly obtained. Because X and Y are defined (see Equations [19] and [20]) as the magnetization vectors of the water and fat, respectively, the correct solution should have Y with a leading phase relative to X. The phase relationship can be checked when X and Y are not exactly anti-symmetric (e.g., $\alpha \neq 180°$). Another requirement is that both X and Y should have measurable amplitudes (i.e., appreciable amounts of both water and fat should exist in a pixel). (Reprinted from Xiang and An (16) with permission of Wiley-Liss, Inc, a subsidiary of John Wiley & Sons.)

$$\Delta S = \frac{\sqrt{(e^{i\alpha} + 1)^2 S_1^2 - 4e^{i\alpha} S_0 S_2}}{e^{i\alpha} - 1} \qquad [23]$$

The two sets of solutions in Equations [21]–[22] are symmetrically related to each other by a simple exchange, i.e., $X_1 = Y_2$ and $Y_1 = X_2$ (Fig. 5). Obviously, only one of the two solutions can be physically correct. DPE makes a selection from the two solutions by comparing the relative phase angle between X and Y. According to the definition in Equations [19]–[20], the physically correct solution should have Y with a leading phase relative to X because of the fact that fat has a lower resonant frequency than water. Thus, DPE can correctly determine water and fat on a pixel basis without the actual determination of the phase angle ϕ or ϕ_0.

Two conditions must be met for DPE to reliably determine the relative phase between X and Y that serves as the basis for the correct water and fat separation. The first requirement can be easily satisfied in the data acquisition and specifies that α should not be 180°, or an angle for which water and fat are exactly anti-symmetric. The second requirement is that any pixel with a signal should have appreciable amounts of both water and fat. If one of the components is absent or negligibly small, the relative phase becomes indeterminate. Unfortunately, a majority of the tissues in vivo are either water dominant or fat dominant. For these pixels, the water and fat separation on the basis of the relative phase angle is problematic. To resolve these "single peak" pixels, DPE relies on an additional processing step that uses a special region growing algorithm. According to the algorithm (16), an orientation vector is defined from X and Y. Regardless of whether a pixel contains a single component or both water and fat, the orientation vector is parallel to the direction defined by the magnetic field inhomogeneity if the correct solution for X and Y is selected. If the alternative and the physically incorrect solution for X and Y is selected, the orientation vector will point to a direction that is different from the direction defined by the magnetic field inhomogeneity. For example, the incorrect orientation vector will have a 90° deviation if the (0, 90°, 180°) sampling scheme is used.

In DPE, the special region growing is invoked repeatedly from multiple randomly selected initial seed pixels to derive an orientation vector field that is spatially smooth in its direction (16). The results for a given pixel from different rounds of the region growing are recorded, and the final decision for a given pixel on its correct orientation vector (and the water and fat assignment) is based on a majority "vote." The pixel-based relative phase analysis of DPE is used to provide a statistical bias for the region growing. This is important for the "voting" mechanism because the success of the final results depends on the assumption that at the beginning of the region growing, the number of the pixels with the correct water and fat separation is more than the number of the pixels with the incorrect water and fat separation (16). DPE has been reported successful for many clinical patient images and robust even in the presence of large motion artifacts (16,17). However, the overall processing used in DPE, particularly the region growing, is quite elaborate and the processing time can be long. As for the region growing by Szumowski et al, DPE also requires an empirical angular threshold (e.g., $\pm 10°$) and thus suffers from the same limitations in the critical step of selecting one of the two possible candidates as the correct orientation vector for each pixel.

Another analytical method for water and fat separation is to acquire three or more separate images with different water and fat relative phase angles and to determine the water and fat on a pixel basis through an iterative least-squares process (18). In this approach, an initial guess for the phase error ϕ is first specified for each pixel. In the original implementation, $\phi = 0$, which corresponds to a uniform magnetic field, is first assumed for all the pixels. With ϕ being known, Equation [1] becomes linear in W and F, and thus the problem of determining W and F becomes amenable to the standard linear least-squares fitting. Once W and F are determined, they can be substituted back into Equation [1] to obtain a new set of linear equations in ΔW, ΔF, and $\Delta\phi$, which represent the deviation of W, F, and ϕ from their true values. These linear equations can again be solved with the linear least-squares fitting, and such a process can be iterated until a predetermined condition (e.g., $\Delta\phi$ is less than a preset value) is met.

Theoretically, the linear least-squares approach can be applied to any three or more images with flexible relative water/fat phase angles. However, the cost function used in the fitting process may contain different minima and, as a result, the fitting process can have multiple solutions. If the initial value for ϕ is close to a local minimum, the fitting process will likely converge to an incorrect solution. It can be shown that for the "single peak" pixels, Equation [1] has an intrinsic am-

biguity with two sets of possible solutions (19). Even for pixels with a mixture of both water and fat, the cost function used for the linear least-square fitting usually contains multiple local minima. Therefore, the iterative process by itself may converge to the incorrect solution for W and F if the initial guess for ϕ is not close to its true value. As an improvement, a region growing algorithm has been proposed to generate a more accurate initial guess for ϕ before the iterative process is applied (19). The region growing used in Yu et al (19) starts from an initial seed pixel that has a "median" value of ϕ among all the pixels based on an initial round of iterative processing with $\phi = 0$. The region growing then propagates to the rest of the image in a predetermined square-spiral trajectory. For each pixel during the region growing, the initial guess for the phase of the pixel is determined from a local two-dimensional linear extrapolation. The integration of the region growing and the iterative linear least-squares methods has been reported to generate substantially improved results compared with using the original iterative process alone (19).

In addition to DPE and the iterative least-squares methods, other pixel-based analytical methods for water and fat separation have also been reported. For three-point Dixon data acquired at (0, 180°, 360°) phase angles, Wang et al proposed using a set of phase consistency conditions to detect the presence of phase wrapping on a pixel basis (20). If the relative phase between the two images with the 0 and 360° phase angles exceeds the condition, phase wrapping is deemed to have occurred and a 360° phase will be either added or subtracted to the 360° image for phase unwrapping. Another analytical approach for processing the three-point Dixon data on a pixel basis is through a modification of the harmonic retrieval (HR) framework (21). The HR framework is well established and widely used in the field of spectral analysis to estimate unknown frequencies from a time-domain signal (22). For Dixon processing, the HR framework can be adapted to determine the field inhomogeneity with the constraint that the frequency difference between water and fat is a known constant. Compared with the iterative least-squares approach, the HR framework allows a priori determination of all the feasible solutions to the field map. The correct field map can then be selected by imposing the "spatial smoothness" condition. A fundamental difficulty with the method, as well as all other pixel-based analytical methods, is that it can not handle directly the "single peak" pixels. As a result, the final success is always dependent on some additional processing, such as by a region-growing algorithm. Finally, a major practical limitation of all the pixel-based methods is that they require a minimum of three sets of acquired images for correct processing.

THE EXTENDED TWO-POINT DIXON TECHNIQUES

While many efforts have been made to develop a robust three-point Dixon technique following the original Dixon paper, many investigators realized that substantial redundancy exists in the data from a three-point Dixon acquisition. Coombs et al (23) and Skinner and Glover (24) pointed out that correction of the field inhomogeneity effects can be achieved with the data from only a two-point acquisition. To see this is indeed possible, Equations [4–5] can be used to derive the field inhomogeneity-related phase as follows:

$$\hat{\phi} = 0.5 \cdot \arg\{(S_1 \cdot S_0^*)^2\} \qquad [24]$$

Comparison to Equation [11] illustrates that as long as W and F are not exactly equal, the square operation in Equation [24] practically synthesizes the signal equivalent to that acquired when the water and fat are 360° in phase. When W and F are exactly equal, S_1 becomes zero and the phase in Equation [24] is indeterminate. However, because S_1 is zero, calculation of W and F is independent of its phase. As far as water and fat separation is concerned, the data from a two-point acquisition are, therefore, sufficient for practically all the situations.

As for the three-point Dixon data, the main challenge in a three-point Dixon technique lies in determining the field inhomogeneity-related phase error, such as by Equation [24]. In fact, many phase-correction algorithms developed for the three-point Dixon processing, such as phase unwrapping by means of polynomial fitting (25), region growing (23,26) or solving the Poisson equations (24,27), were applied almost directly to the processing of the two-point Dixon data. For actual applications, however, phase unwrapping has been found to be more error-prone with the two-point Dixon data than with the three-point Dixon data. The decreased processing reliability is often a result of the signal cancellation in pixels where water and fat coexist, particularly along the boundaries of water-dominant and fat-dominant regions. Although phase determination is unimportant for pixels where water and fat signals are exactly equal, phase uncertainty for these pixels and increased phase variation for pixels where water and fat are only partially cancelled can pose great challenge for many phase unwrapping algorithms that require an empirical angular threshold as a criteria for phase unwrapping. As discussed above, it can be very difficult or even impossible to find an optimal angular threshold that can avoid either artificially segmenting the image or compromising the reliability of the phase unwrapping.

Whether it is for three-point or two-point Dixon processing, it is interesting to note that determining $e^{i\phi}$ (which is sometimes referred as phase vector or phasor) alone without an explicit determination of ϕ is sufficient for correct water and fat separation. In the complex plane, phase vector represents a unit vector whose direction is determined by ϕ but unaffected by a possible phase wrap in ϕ. Because ϕ is spatially smooth, the direction represented by the phase vector should also be smooth. For the two-point Dixon data, it is easy to show from Equations [4] and [5] that the phase vector is equal to $\frac{S_1 \cdot S_0^*}{|S_1| \cdot S_0}$ for water-dominant ($W > F$) pixels and $-\frac{S_1 \cdot S_0^*}{|S_1| \cdot S_0}$ for fat-dominant ($W < F$) pixels. Therefore, the phase vector is directly derivable from S_0 and S_1 to

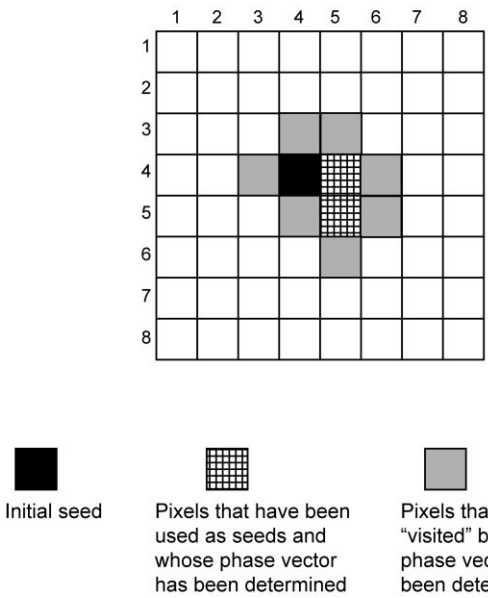

Pixel stacks	Sequence of populating the pixel stacks
#1	(4,4) (5,4) (4,4) (5,6)
#2	(5,5) (5,4)
#3	(6,4) (4,5)
#4	(4,5)
....	
#16	(4,3)
#17	(5,3)
#18	(3,4) (6,5)

Figure 6. A region-growing scheme used for phase correction in a two-point Dixon technique. The initial seed pixel can be selected randomly or with other more judicious criteria. The determination of the growth sequence is facilitated by multiple pixel stacks. According to the scheme, a pixel with smaller (larger) phase difference is placed onto a lower (higher) order pixel stack. Pixels placed onto the lower-order pixel stacks will be "grown" before the pixels placed onto the higher-order stacks. Good and stable regions are thus processed before bad and noisy regions. Use of the multiple pixels avoids the need for an empirical angular threshold that is used for most other region-growing algorithms. Additionally, the region growing can even recover from some local errors because it does not need to be spatially contiguous.

within a + or − sign. Note that the change in the phase vector direction is not related to phase wrapping. However, the choice between the + or − sign for the phase vector can be detected as an abrupt change in the direction of the phase vector and, therefore, achieved similarly as for phase unwrapping. Exploiting this fact, Akkerman and Maas (28) used a region-growing algorithm similar to that used by Szumowski et al (15) and showed that water and fat separation can be successfully achieved for a two-point Dixon data without direct phase unwrapping.

A different region-growing algorithm that aims also at determining the phase vector rather the phase for water and fat separation from a two-point Dixon data was proposed by Ma (29). Compared with previously reported algorithms, this algorithm has several important improvements. First, the initial seed pixel can be randomly selected rather than relying on manual selection. Second, the selection of the correct phase vector for each seed pixel is based on a local expectation value rather than a single neighboring pixel. The local expectation value is calculated using both the amplitude and the phase vector of the neighboring pixels. As a result, the region growing can continue uncorrupted in regions of low signal (such as the water/fat boundary pixels) or artifacts. Third, the sequence of the region growing follows an order of the minimum phase difference (30–32) by which "good" regions of small phase variations are grown before "bad" regions of large phase variations. The determination of the growth sequence is facilitated by the use of the multiple pixel stacks (Fig. 6). At each step of the region growing, the nearest neighbor pixels of the seed pixel are consecutively placed onto one of the pixel stacks according to the phase difference between the seed pixel and its nearest neighbor pixels. If the phase difference is small, the nearest neighbor pixel will be placed onto a low-order pixel stack. Conversely, the nearest neighbor pixel will be placed onto a higher-order pixel stack if the phase difference is large. Pixels that are placed on the lower-order pixel stacks are assigned higher priority and will be grown before the pixels that have been placed on the higher-order pixel stacks. Note that because of the use of the multiple pixel stacks, the region growing does not require an empirical angular threshold for the critical step of determining the phase vector for each pixel. Furthermore, the actual region growing does not need to be spatially contiguous and thus can even recover from isolated local errors.

As another variation to the original two-point Dixon technique, Xiang recently reported a two-point Dixon technique that accommodates acquisition of an in-phase image and a partially opposed-phase image (where water and fat signals are not exactly at 180°) (33). On the basis of the in-phase and partially opposed-phase images, two phasor candidates can be computed for every pixel. The two phasor candidates are somewhat analogous to the two phase vectors with a + and a − sign for the symmetrically acquired two-point Dixon technique. The phasor that provides the correct water and fat separation is spatially smooth in its direction and is derived in a regional iterative phasor extraction (RIPE) algorithm. According to Xiang (33), RIPE is an implementation of "cellular automata," which in general can be used to establish a long-range global structure from the collective effects of a large

number of local entities (i.e., phasors for each pixel in this case). In the cellular automata framework, each of the local entities may vary simultaneously according to some simple rules. Cellular automata may be applicable to Dixon imaging because the essential objective of phase unwrapping or RIPE is to detect and remove the local discontinuity in the wrapped phase or the phasor directions (34). Because the final result is reached from collective and simultaneous interactions of all the pixels, the application of the cellular automata has a potential advantage of path independence. However, there is less tractability compared with the path-following methods, and there is no guarantee that the long-range structure after the cellular automata processing is truly correct (34).

THE SINGLE-POINT DIXON TECHNIQUES

By eliminating the need for the acquisition of a third data point, a two-point Dixon technique provides a substantial improvement in data acquisition efficiency. Because an MR image is in general complex and contains both real and imaginary channels, it is possible in an ideal situation to place water and fat into the separate channels and achieve water and fat separation from a single-point acquisition when the water and fat are acquired in quadrature (i.e., at a 90° relative phase angle) (35–38). In reality, phase errors are unavoidable, and the real and imaginary channels of an MR image will always contain a mixture of both water and fat. Generally speaking, the signal from a single acquisition by Equation [1] has three unknown variables (W, F, and $\phi + \phi_0$). Therefore, there is not enough information to remove the phase error term $\phi + \phi_0$ to achieve the desired water and fat separation. Most of the previously reported phase correction methods for a single-point Dixon technique thus rely on using additional data from reference scans (35,36,39,40) or on using empirical phase modeling (37,38).

A phase-correction method for a single-point Dixon technique without requiring any reference scans or explicit modeling of the phase errors has been reported by Xiang (41,42). The method works by first applying a heavy low-pass filtering to the complex image from a single-point quadrature acquisition. Pixels with a significant signal reduction after the filtering are identified and assumed as the water/fat boundary pixels. Regions segmented by the boundary pixels are then classified as water-dominant or fat-dominant regions by examining the phase of the boundary pixels. In his initial report, Xiang applied an empirical 78° rotation to the signals in all the fat region pixels (41). A subsequent improvement was made with "virtual shimming," in which the phase angle of the rotation is adaptively adjusted for different fat regions to maximize the total signal after phase correction (42).

Under an explicit initial assumption that all the pixels with appreciable amount of signals are either water dominant or fat dominant, phase correction for data from a strictly single-point Dixon acquisition can also be achieved with a region-growing process (43,44). When this assumption is valid, the direction related to the phase of the signal is expected to be smooth throughout the image, except for the pixels along the interface between the water-dominant and fat-dominant regions. A region-growing process guided by the phase gradients and similar to that for a two-point Dixon phase correction (29) can be used to detect and correct these directional changes and, therefore, permit water/fat separation using a strictly single-point Dixon image. The initial assumption that all the pixels are either water dominant or fat dominant can be relaxed by low-pass filtering the phase vector map that is determined from the region growing (44). An advantage of the method is that the algorithm can be fully automated and naturally extended to data acquired with a flexible echo time, including those sampled at a phase angle that is not exactly in quadrature (44).

THE DATA ACQUISITION STRATEGY AND OTHER CONSIDERATIONS

Dixon techniques can be successfully implemented with many different pulse sequences, including fast spin echo (18,45–48), steady-state free precession (18,49), or even non-rectilinear (50,51) pulse sequences. However, the success of most Dixon techniques is in general dependent on the success of phase correction. Failure in phase correction usually leads directly to swapped water and fat assignment for the pixels affected. Another factor that can significantly affect the overall performance of a Dixon technique is the data acquisition strategy (which is often dictated by a specific phase correction algorithm) and how the data acquisition strategy is implemented for a specific pulse sequence. A data acquisition or an implementation that requires a long scan time, for example, could increase the severity of motion-related artifacts, which is an important source of challenge for phase correction. Additionally, the relative water/fat phase angles required by a phase-correction algorithm may also be important. Because most modern pulse sequences are designed for maximum time efficiency and optimal image quality, changes in the pulse sequence timing to effect the desired water/fat phase angles (e.g., echo time in a gradient echo or echo spacing in a fast spin echo pulse sequence) will usually reduce the scan time efficiency and/or degrade the image quality (e.g., lower SNR or increased blurring due to increased signal relaxation). Thus, a data acquisition with the smallest water/fat phase angle changes would be ideal. However, the success of phase correction essentially depends on the ability to detect and correct the induced phase angle changes in the presence of noise and other phase perturbations. Therefore, images acquired with small phase angle changes (even when they are theoretically allowed by a phase correction algorithm) will likely provide insufficient processing reliability. In addition, small water/fat phase angle changes in the acquired images usually will result in poor SNR for the processed water-only and fat-only images. Therefore, the phase correction algorithm, the data acquisition strategy, and its implication for the quality of the acquired and processed images must all be carefully considered in selecting or evaluating a Dixon technique.

From a scan time perspective, a single-point Dixon technique obviously requires the shortest scan time. A strictly single-point Dixon technique, however, generally does not have sufficient information for water/fat separation and must make an essential a priori assumption that a pixel is either water dominant or fat dominant. Although this assumption can be relaxed in the processing to achieve good qualitative fat suppression, a strictly single-point Dixon technique cannot be exactly quantitative for all possible applications. A single-point Dixon technique that requires a reference scan for phase error determination will increase the overall scan time. More importantly, acquiring a reference scan will always open the possibility for potential degradations from patient motion or scanner instability. Compared with a single-point Dixon acquisition or an acquisition by a non-Dixon technique, a two-point Dixon acquisition typically results in a doubling of the minimum scan time. However, a two-point Dixon acquisition saves one third of the time relative to a three-point Dixon acquisition. As far as water/fat separation is concerned, a two-point Dixon acquisition provides essentially the same information as a three-point Dixon acquisition, except for pixels with equal amounts of water and fat. With a careful design in the phase-correction algorithm, these exceptions can easily be handled properly. Generally speaking, shorter scan time reduces the potential for motion-related artifacts (e.g., ghosting, blurring, and image mis-registration), which are always potential sources for processing failure. From the perspective of water and fat separation, a two-point Dixon technique is, therefore, always more advantageous than a three-point Dixon technique when the phase correction is not affected by the presence of the pixels where water and fat are comparable.

Several methods can be used either alone or in combination to reduce the scan time of a Dixon acquisition. Most of these techniques are applicable to the different sampling strategies and/or different pulse sequence implementations of a Dixon technique. For data acquired with multiple receiver coils, partially parallel imaging (PPI) can reduce the scan time of a non-Dixon acquisition by a factor up to the number of the coils through *k*-space undersampling (52,53). PPI is equally effective in reducing the scan time of a Dixon acquisition, because the same PPI processing is usually applied to each individual Dixon image. As a result, the relative phase between the different acquired images and the ability to separate water and fat are not affected. The combination of a Dixon technique with PPI was demonstrated first for a fast spin echo three-point Dixon acquisition (54) and later in several other Dixon implementations (55,56). These implementations showed that PPI and Dixon processing are mutually complementary in scan time and SNR. Ignoring the effect of the coil geometric factors, the SNR loss in PPI due to the scan time reduction can be compensated for by the SNR gain from a Dixon technique due to the multiple point acquisition. A second method that is effective in reducing the minimum scan time of a Dixon acquisition is to acquire the multiple input images with dual-echo (29,57) or multi-echo (48,58,59) readouts. Dual-echo and multi-echo readouts can use either gradients of alternating polarity for minimum dead-time in a pulse sequence or gradients of the same polarity with additional "flyback" rewinder gradients. Compared with a conventional sequential or interleaved multiple-point Dixon acquisition, dual-echo or multi-echo readouts can save scan time substantially and greatly minimize the spatial mis-registration or ghosting artifacts due to motion. Because a Dixon technique usually requires a specific relative phase angle between the input images, dual-echo or multi-echo readouts often require a specific interecho spacing, which in turn may place a limit on the number of the readout points and/or the receiver bandwidth that can be prescribed (particularly at a higher field strength such as 3.0 Tesla). With modern high-powered gradients and fast receivers, however, the desired echo spacing can usually be accommodated by increasing the receiver bandwidth. For most practical applications, the high receiver bandwidth can actually be advantageous because it entails less T2*-related signal loss and less image blurring. A third method that has been used for reducing the scan time is partial *k*-space acquisition and homodyne image reconstruction (60). The underlying requirement for the homodyne reconstruction is that the object to be imaged is real and has no imaginary component. For Dixon imaging, this requirement is met when the water and fat signals are sampled exactly in phase or 180° out of phase. Therefore, Dixon techniques requiring only the in-phase and 180° out-of-phase images are directly amenable to homodyne processing (46,61). When water and fat signals are not in-phase or 180° out-of-phase, the underlying object is generally not real and has an imaginary component. Nevertheless, application of the homodyne reconstruction in some of the more general cases has also been shown and reported (62).

A different and less-noted implication of the Dixon acquisitions on the scan time and image quality arises from the need to vary the echo times from those of a non-Dixon acquisition. As stated above, the gradient and RF pulses and data acquisition window of many modern fast pulse sequences are usually packed as tightly as allowed by the underlying imaging principles to achieve the best image quality and the shortest total scan time. Changing the echo times as required by a Dixon acquisition often necessitates some compromises to the optimal pulse sequence design (e.g., by increasing the minimum echo time and minimum sequence repetition time for the fast gradient echo pulse sequence, or by increasing the minimum interecho spacing for the fast spin echo pulse sequence). These compromises may have a substantial effect on the image quality and lead to either some additional increase to the minimum total scan time or a sizable loss to the total number of slices allowed within a given sequence repetition time. With careful pulse sequence design and choice in image reconstruction algorithms, these drawbacks can also be successfully managed (46,48,63).

As well recognized, an increased number of sampling in a Dixon technique in general leads to an increased SNR in the processed water-only and fat-only images when compared with an individual acquired image. The SNR efficiency of a Dixon technique can be characterized with the number of signal average (NSA), which is defined (8) as:

$$NSA = \frac{\sigma_0^2}{\sigma_{w,f}^2} \quad [25]$$

where σ_0^2, $\sigma_{w,f}^2$ represent the noise variance for one of the acquired images and for the processed water (or fat)-only image, respectively. The NSA value of a Dixon technique is dependent on the sampling strategy as well as on the processing scheme. For the three-point Dixon data sampled at (0, α, 2α), a maximum NSA of 3 is achieved when $\alpha = 120°$ (8,16). When $\alpha \neq 120°$, NSA is generally less than 3. Similarly, a maximum NSA of 2 is achieved for the two-point Dixon data sampled at (0, α) only when $\alpha = 180°$ (29,33).

Using a Cramer-Rao bound analysis on three-point Dixon data, Pineda et al found that the SNR performance can also be dependent on the relative amount of water and fat in a pixel (64). According to their analysis, the maximum NSA of 3 is achieved uniformly for all the possible water/fat ratios only when the data are sampled at ($-30° + k\cdot 180°$, $90° + k\cdot 180°$, $210° + k\cdot 180°$), where k is an integer. For other sampling schemes such as the symmetric sampling at ($-\alpha$, 0, α), NSA is found to be in general dependent on the water/fat ratio. In particular, NSA becomes zero for water-only and fat-only images when water and fat are equal. The SNR performance from this analysis forms the basis for the IDEAL (iterative decomposition of water and fat with echo asymmetry and least-squares estimation) technique (65,66). The essential component of the IDEAL technique is the combination of the iterative least-squares approach for water/fat separation (18) and the optimal sampling scheme under which NSA is independent of the water/fat ratios. It is important to point out, however, that the results from the Cramer-Rao analysis are valid only when the field inhomogeneity-related phase error, water, and fat are all estimated together on a pixel-by-pixel basis (64,67). When the field inhomogeneity-related phase error is known or determined separately by phase correction, the NSA for the water-only and fat-only images easily becomes independent of the water/fat ratio and in fact can surpass the upper limit that is predicted by the Cramer-Rao bound analysis (64,67).

CONCLUSIONS

For a two-component system consisting of only water and fat, the Dixon techniques represent the simplest and most efficient implementation of the more general spectroscopic imaging (68,69). However, the omnipresence of the phase errors, noise, and artifacts in an MR image, as well as the special case of the "single peak" pixels, can make a general solution to the problem extremely challenging. The most critical step for the success of any Dixon techniques is the phase correction in postprocessing, which universally relies on an assumption that the underlying phase errors (excluding the effect of noise and artifacts) are spatially smooth. The strategy and implementation of the data acquisition strategy can also have a great impact on the reliability of the phase correction and the quality of the processed water-only and fat-only images. Despite these challenges, tremendous technical developments have been made over the last two decades. It is now clear that for many clinical applications, Dixon techniques can be used for water and fat imaging more reliably, with better image quality, and in a similar or even shorter scan time than the other more conventional techniques.

In addition to water and fat imaging, a byproduct of many Dixon techniques is the magnetic field map, which is directly related to the phase map after phase unwrapping and useful for field shimming and other purposes (12). Some Dixon techniques may also be helpful in the assessment of the tissue iron concentration through the determination of transverse relaxation times (8,59,70). Furthermore, many phase-correction algorithms used for a Dixon technique can be extended directly to imaging of silicone implants (71–73) or other phase-sensitive MRI techniques such as phase-sensitive inversion recovery imaging (74,75). With the continued technical development of the Dixon techniques and their introduction into the product by some major MR vendors, we firmly believe that these techniques will become an increasingly important tool for both clinical and research applications in MRI.

REFERENCES

1. Frahm J, Haase A, Hanicke W, et al. Chemical shift selective MR imaging using a whole-body magnet. Radiology 1985;156:441–444.
2. Bydder GM, Young IR. MR imaging: clinical use of the inversion recovery sequence. J Comput Assist Tomogr 1985;9:659–675.
3. Dixon WT. Simple proton spectroscopic imaging. Radiology 1984; 153:189–194.
4. Low RN, Knowles A, Vu AT, Slavens Z, Estowski L. LAVA dual echo with water reconstruction: preliminary experience with a novel pulse sequence for gadolinium-enhanced abdominal MR imaging. In: Proceedings of the 15th Annual Scientific Meeting of the ISMRM, Berlin, Germany, 2007. (abstract 726).
5. Kuroda K, Oshio K, Mulkern RV, Jolesz FA. Optimization of chemical shift selective suppression of fat. Magn Reson Med 1998;40: 505–510.
6. Yeung HN, Kormos DW. Separation of true fat and water images by correcting magnetic field inhomogeneity in situ. Radiology 1986; 159:783–786.
7. Glover GH, Schneider E. Three-point Dixon technique for true water/fat decomposition with B0 inhomogeneity correction. Magn Reson Med 1991;18:371–383.
8. Glover GH. Multipoint Dixon technique for water and fat proton and susceptibility imaging. J Magn Reson Imaging 1991;1:521–530.
9. Ghiglia DC, Pritt MD. Two-dimensional phase unwrapping: theory, algorithms, and software. New York: John Wiley & Sons; 1998.
10. Chavez S, Xiang QS, An L. Understanding phase maps in MRI: a new cutline phase unwrapping method. IEEE Trans Med Imaging 2002;21:966–977.
11. Song SM, Napel S, Pelc NJ, Glover GH. Phase unwrapping of MR phase images using Poisson equation. IEEE Trans Image Process 1995;4:667–676.
12. Schneider E, Glover G. Rapid in vivo proton shimming. Magn Reson Med 1991;18:335–347.
13. Liang ZP. A model-based method for phase unwrapping. IEEE Trans Med Imaging 1996;15:893–897.
14. Goldstein RM, Zebker HA, Werner CL. Satellite radar interferometry: two-dimensional phase unwrapping. Radio Sci 1988;23:713–720.
15. Szumowski J, Coshow WR, Li F, Quinn SF. Phase unwrapping in the three-point Dixon method for fat suppression MR imaging. Radiology 1994;192:555–561.
16. Xiang QS, An L. Water-fat imaging with direct phase encoding. J Magn Reson Imaging 1997;7:1002–1015.

17. Rybicki FJ, Mulkern RV, Robertson RL, Robson CD, Chung T, Ma J. Fast three-point Dixon MR imaging of the retrobulbar space with low-resolution images for phase correction: comparison with fast spin-echo inversion recovery imaging. AJR Am J Neuroradiol 2001; 22:1798–1802.
18. Reeder SB, Wen Z, Yu H, et al. Multicoil Dixon chemical species separation with an iterative least-squares estimation method. Magn Reson Med 2004;51:35–45.
19. Yu H, Reeder SB, Shimakawa A, Brittain JH, Pelc NJ. Field map estimation with a region growing scheme for iterative 3-point water-fat decomposition. Magn Reson Med 2005;54:1032–1039.
20. Wang Y, Li D, Haacke EM, Brown JJ. A three-point Dixon method for water and fat separation using 2D and 3D gradient-echo techniques. J Magn Reson Imaging 1998;8:703–710.
21. Jacob M, Sutton BP. Non-iterative decomposition of fat and water using chemical shift. In: Proceedings of the 16th Annual Scientific Meeting of the ISMRM, Berlin, Germany, 2007. (abstract 1630).
22. Stoica P, Moses R. Introduction to spectral analysis. Upper Saddle River, NJ: Prentice Hall; 1997.
23. Coombs BD, Szumowski J, Coshow W. Two-point Dixon technique for water-fat signal decomposition with B0 inhomogeneity correction. Magn Reson Med 1997;38:884–889.
24. Skinner TE, Glover GH. An extended two-point Dixon algorithm for calculating separate water, fat, and B0 images. Magn Reson Med 1997;37:628–630.
25. Yang GZ, Firmin DN, Mohiaddin RH, Konrad JP, Longmore. DB. B0 inhomogeneity correction for two-point Dixon chemical shift imaging. In: Proceedings of the 11th Annual Scientific Meeting of the SMRM, Berlin, Germany, 1992. (abstract 3819).
26. Coombs BD, Szumowski J, Coshow W, Li F. Two-point Dixon technique for water-fat signal decomposition with B0 inhomogeneity correction. In: Proceedings of the 3rd Annual Scientific Meeting of the Society of Magnetic Resonance, Nice, France, 1995. (abstract 647).
27. Zhu G, Huang J, Hariharan H, Freeland S. A robust water and fat separation method. In: Proceedings of the 4th Annual Scientific Meeting of the ISMRM, San Francisco, California, USA, 1995. (abstract 1542).
28. Akkerman EM, Maas M. A region-growing algorithm to simultaneously remove dephasing influences and separate fat and water in two-point Dixon imaging. In: Proceedings of the 3rd Annual Scientific Meeting of the ISMRM, Nice, France, 1995. (abstract 649).
29. Ma J. Breath-hold water and fat imaging using a dual-echo two-point Dixon technique with an efficient and robust phase-correction algorithm. Magn Reson Med 2004;52:415–419.
30. Ching NH, Rosenfeld D, Braun M. Two-dimensional phase unwrapping using a minimum spanning tree algorithm. IEEE Trans Image Process 1992;1:355–365.
31. An L, Xiang QS, Chavez S. A fast implementation of the minimum spanning tree method for phase unwrapping. IEEE Trans Med Imaging 2000;19:805–808.
32. Christofides N. Graph theory: an algorithmic approach. New York: Academic Press; 1975.
33. Xiang QS. Two-point water-fat imaging with partially-opposed-phase (POP) acquisition: an asymmetric Dixon method. Magn Reson Med 2006;56:572–584.
34. Ghiglia DC, Mastin GA, Romero LA. Cellular-automata method for phase unwrapping. J Opt Soc Am A Opt Image Sci Vis 1987;4:267–280.
35. Paltiel Z, Ban A. Separate water and lipids images obtained by a single scan. In: Proceedings of the 4th Annual Scientific Meeting of the SMRM, London, England, 1985. (abstract 172).
36. Patrick J, Haacke E, Hahn J. Separate water and lipids images obtained by a single scan. In: Proceedings of the 4th Annual Scientific Meeting of the SMRM, London, England, 1985. (abstract 174).
37. Ahn CB, Lee SY, Nalcioglu O, Cho ZH. Spectroscopic imaging by quadrature modulated echo time shifting. Magn Reson Imaging 1986;4:110–111.
38. Hajnal J, Young I. Use of spatial phase distribution models to produce water and fat only images from single echo shifted data sets. In: Proceedings of the 4th Annual Scientific Meeting of the ISMRM, San Francisco, California, USA, 1995. (abstract 650).
39. Ma J. Multipoint Dixon imaging with reduced time and increased reliability. In: Proceedings of the 6th Annual Scientific Meeting of the ISMRM, Sydney, Australia, 1998. (abstract 622).
40. Yu H, Reeder SB, McKenzie CA, et al. Single acquisition water-fat separation: feasibility study for dynamic imaging. Magn Reson Med 2006;55:413–422.
41. Xiang QS. Fat suppression with single quadrature acquisition. In: Proceedings of the 6th Annual Scientific Meeting of the ISMRM, Sydney, Australia, 1998. (abstract 1880).
42. Xiang QS. Improved single point water-fat imaging with virtual shimming. In: Proceedings of the 9th Annual Scientific Meeting of the ISMRM, Glasgow, Scotland, 2001. (abstract 789).
43. Son J, Ji J, Ma J. Three-dimensional T1-weighted MR imaging using a one-point Dixon technique with arbitrary echo times. In: Proceedings of the 13th Annual Scientific Meeting of the ISMRM, Miami, Florida, USA, 2005. (abstract 893).
44. Ma J. A single-point dixon technique for fat-suppressed fast 3D gradient-echo imaging with a flexible echo time. J Magn Reson Imaging 2008;27:881–890.
45. Hardy PA, Hinks RS, Tkach JA. Separation of fat and water in fast spin-echo MR imaging with the three-point Dixon technique. J Magn Reson Imaging 1995;5:181–185.
46. Ma J, Singh SK, Kumar AJ, Leeds NE, Broemeling LD. Method for efficient fast spin echo Dixon imaging. Magn Reson Med 2002;48: 1021–1027.
47. Ma J, Singh SK, Kumar AJ, Leeds NE, Broemeling LD. Phased array coil compatible T2-weighted fast spin echo Dixon imaging. In: Proceedings of the 10th Annual Scientific Meeting of the ISMRM, Hawaii, USA, 2002. (abstract 735).
48. Ma J, Son JB, Zhou Y, Le-Petross H, Choi H. Fast spin-echo triple-echo Dixon (fTED) technique for efficient T2-weighted water and fat imaging. Magn Reson Med 2007;58:103–109.
49. Huang TY, Chung HW, Wang FN, Ko CW, Chen CY. Fat and water separation in balanced steady-state free precession using the Dixon method. Magn Reson Med 2004;51:243–247.
50. Moriguchi H, Lewin JS, Duerk JL. Dixon techniques in spiral trajectories with off-resonance correction: a new approach for fat signal suppression without spatial-spectral RF pulses. Magn Reson Med 2003;50:915–924.
51. Moriguchi H, Lewin JS, Duerk JL. Fast Spiral two-point Dixon technique using block regional off-resonance correction. Magn Reson Med 2004;52:1342–1350.
52. Sodickson DK, Manning WJ. Simultaneous acquisition of spatial harmonics (SMASH): fast imaging with radiofrequency coil arrays. Magn Reson Med 1997;38:591–603.
53. Pruessmann KP, Weiger M, Scheidegger MB, Boesiger P. SENSE: sensitivity encoding for fast MRI. Magn Reson Med 1999;42:952–962.
54. Ma J, Bankson JA, Stafford RJ. Multipoint Dixon imaging using sensitivity encoding. In: Proceedings of the 11th Annual Scientific Meeting of the ISMRM, Toronto, Canada, 2003. (abstract 1068).
55. McKenzie CA, Reeder SB, Shimakawa A, Pelc NJ, Brittain J. Abdominal three-point Dixon imaging with self-calibrating parallel MRI. In: Proceedings of the 12th Annual Scientific Meeting of the ISMRM, Kyoto, Japan, 2004. (abstract 917).
56. Ma J, Son JB, Bankson JA, Stafford RJ, Choi H, Ragan D. A fast spin echo two-point Dixon technique and its combination with sensitivity encoding for efficient T2-weighted imaging. Magn Reson Imaging 2005;23:977–982.
57. Ma J, Vu AT, Son JB, Choi H, Hazle JD. Fat-suppressed three-dimensional dual echo dixon technique for contrast agent enhanced MRI. J Magn Reson Imaging 2006;23:36–41.
58. Reeder SB, Vu AT, Hargreaves BA, et al. Rapid 3D-SPGR imaging of the liver with multi-echo IDEAL. In: Proceedings of the 14th Annual Scientific Meeting of the ISMRM, Seattle, Washington, USA, 2006. (abstract 2444).
59. Ma J, Wehrli FW, Song HK, Hwang SN. A single-scan imaging technique for measurement of the relative concentrations of fat and water protons and their transverse relaxation times. J Magn Reson 1997;125:92–101.
60. Noll DC, Nishimura DG, Macovski A. Homodyne detection in magnetic resonance imaging. IEEE Trans Med Imaging 1991;10:154–163.
61. Ragan DK, Ma J. A hybrid homodyne algorithm for reconstructing partially acquired two-point Dixon data. In: Proceedings of the 14th Annual Scientific Meeting of the ISMRM, Seattle, Washington, USA, 2006. (abstract 2967).
62. Reeder SB, Hargreaves BA, Yu H, Brittain JH. Homodyne reconstruction and IDEAL water-fat decomposition. Magn Reson Med 2005;54:586–593.

63. Li Z, Gmitro AF, Bilgin A, Altbach MI. Fast decomposition of water and lipid using a GRASE technique with the IDEAL algorithm. Magn Reson Med 2007;57:1047–1057.
64. Pineda AR, Reeder SB, Wen Z, Pelc NJ. Cramaer-Rao bounds for three-point decomposition of water and fat. Magn Reson Med 2005; 54:625–635.
65. Reeder SB, Pineda AR, Wen Z, et al. Iterative decomposition of water and fat with echo asymmetry and least-squares estimation (IDEAL): application with fast spin-echo imaging. Magn Reson Med 2005;54:636–644.
66. Reeder SB, McKenzie CA, Pineda AR, et al. Water-fat separation with IDEAL gradient-echo imaging. J Magn Reson Imaging 2007; 25:644–652.
67. Pineda AR, Wen Z, Reeder SB, Yu H, Pelc NJ. Cramer-Rao bounds for 3-point Dixon imaging. In: Proceedings of the 12th Annual Scientific Meeting of the ISMRM, Kyoto, Japan, 2004. (abstract 2107).
68. Brown TR, Kincaid BM, Ugurbil K. NMR chemical shift imaging in three dimensions. Proc Natl Acad Sci U S A 1982;79:3523–3526.
69. Sepponen RE, Sipponen JT, Tanttu JI. A method for chemical shift imaging: demonstration of bone marrow involvement with proton chemical shift imaging. J Comput Assist Tomogr 1984;8:585–587.
70. Yu H, McKenzie CA, Shimakawa A, et al. Multiecho reconstruction for simultaneous water-fat decomposition and T2* estimation. J Magn Reson Imaging 2007;26:1153–1161.
71. Schneider E, Chan TW. Selective MR imaging of silicone with the three-point Dixon technique. Radiology 1993;187:89–93.
72. An L, Xiang QS. Chemical shift imaging with spectrum modeling. Magn Reson Med 2001;46:126–130.
73. Ma J, Choi H, Stafford RJ, Miller MJ. Silicone-specific imaging using an inversion-recovery-prepared fast three-point Dixon technique. J Magn Reson Imaging 2004;19:298–302.
74. Xiang QS. Inversion recovery image reconstruction with multiseed region-growing spin reversal. J Magn Reson Imaging 1996;6:775–782.
75. Ma J. Multislice and multicoil phase-sensitive inversion-recovery imaging. Magn Reson Med 2005;53:904–910.